

Molecular Dynamics Studies on Native, Loop-Contracted, and Metal Ion-Substituted Azurins

V. Rajapandian, V. Hakkim, and V. Subramanian*

Chemical Laboratory, Central Leather Research Institute, Council of Scientific and Industrial Research, Adyar, Chennai 600 020, India

Received: November 28, 2009; Revised Manuscript Received: May 12, 2010

Harmonic force field (FF) parameters for the active site of native azurin (AZ) have been developed using density functional theory (DFT)-based Becke's three-parameter hybrid exchange functional and the Lee–Yang–Parr correlation functional (B3LYP) method. The same computational protocol has also been applied to derive the FF parameters for the metal ion-substituted [Co(II) and Ni(II)] AZs. To validate the new set of FF parameters for the metal sites, molecular dynamics (MD) simulations on native, loop-contracted, and metal ion-substituted AZs have been carried out for 10 ns using AMBER parameters for the remaining part of the proteins. The average structure obtained from the MD simulation for native protein is akin to that of X-ray diffraction studies. Results from the *in silico* loop variation reveal that the active site of AZ is almost unaffected by the loop contraction in accordance with the previous experimental findings. However, the inherent hydrogen-bonded network of the metal site of AZ is affected by the loop contraction. Comparison of the average structures obtained from the MD simulations for the metal ion-substituted proteins with the corresponding X-ray diffraction structures shows that there are no major differences between two systems. Nevertheless, the metal ion binding site undergoes significant changes due to metal ion-substitution. Results clearly demonstrate the usefulness of a new set of FF parameters in the engineering and redesign of blue copper proteins.

1. Introduction

Metalloproteins account for nearly half of all proteins in nature.^{1–3} Metal-binding sites are responsible for catalyzing various important biological processes including photosynthesis, respiration, water oxidation, molecular oxygen reduction, and nitrogen fixation.^{1–3} Several studies have been made to understand the structure and function of metalloproteins, as summarized in the recent *Nature Insight*.^{4–7} The ultimate goal is to engineer existing metalloproteins and to design new systems that reproduce the structures and functions of native metalloproteins. Despite the tremendous developments in experimental techniques and computational chemistry methodologies, designing new metalloproteins is a challenging task.^{4–7} From the perspective of computational chemistry, classical mechanics-based force field (FF) simulations such as molecular mechanics (MM) and molecular dynamics (MD) have been employed for this purpose.

There are several MM programs that are capable of being routinely used in the analysis of organic molecules, proteins, and nucleic acids.^{8–10} A variety of FFs have been developed and applied to address different issues in structural biology and biophysical chemistry. Particularly, the success of FF-based methods in the prediction of structure, conformation, folding, and dynamics of proteins and nucleic acids has been well-documented.^{8–10} These methods are also useful to understand the protein–ligand, protein–protein, and protein–nucleic acids interactions; thus, it is possible to gain insight into the *de novo* drug design. Numerous authoritative reviews and books on the applications of FF-based methodology in biological sciences

are available.^{8–23} It is evident from various reports that widely applicable FF parameters for inorganic and bioinorganic systems are not available.^{8–10} The problems in the development of FF parameters for inorganic and bioinorganic systems have been reviewed.^{8–10} Comba et al. have made seminal contributions to the development of inorganic FF.^{16,24–27}

Recently, Zimmer et al. have addressed the question, “Are classical MM calculations still useful in bioinorganic simulations?”^{8–10} In fact, most of the problems mentioned in his earlier review on the development of FF parameters for inorganic and bioinorganic simulations are yet to be resolved completely, viz.: (i) Metal ion systems exist in a variety of coordination numbers (high symmetry around the metal site), oxidation, and spin states; hence, it suffers from the multiple referencing problem. (ii) It is difficult to parametrize the bioinorganic FF parameters from the solid-state structures as there are insufficient high-resolution crystal structures of analogous molecules. (iii) A complete normal-mode analysis has to be carried out for the metal site, or rigid body potential energy surface (PES) scans have to be generated to derive the force constants for the metal site using a reasonably good level of quantum mechanical (QM) calculation. (iv) Deriving the force constants from the experimental IR spectra is difficult because of the low metal ion–ligand [M(II)–L] vibrational frequencies, and their analysis is often complicated by strong electronic effects and by mixing with the ligand vibrational modes. (v) Electronic structure calculations have to be carried out to derive the partial charges corresponding to different oxidation and spin states. (vi) Another important issue is the incorporation of ligand field stabilization energy (LFSE) within the MM framework. Deeth et al. have made significant contributions to the development of ligand field molecular mechanics (LFMM), and it has

* To whom correspondence should be addressed. Tel: +91 44 24411630. Fax: +91 44 24911589. E-mail: subuchem@hotmail.com or subbu@cri.res.in.

been applied to a number of inorganic and bioinorganic systems.^{28–30}

In modeling the inorganic and bioinorganic systems, the utility of electronic structure methods such as ab initio and density functional theory (DFT) approaches has been highlighted in several studies.^{24–27,31–46} However, these methods are not computationally feasible for metalloproteins and metallaenzymes. Hence, the attractive alternative strategies such as QM/MM and ONIOM (our own *N*-layered integrated molecular orbital + MM) approaches have been used to model the bioinorganic systems.^{47–54} The success of the ONIOM method depends on the reliable FF parameters for the metal site. Hence, the development of FF parameters for the metal binding site of metalloproteins is necessary to understand the interrelationships between the structure, function, dynamics, and reactivity. In this context, we have selected azurin (AZ), a member of the blue copper protein family, for the present investigation.

Among the various metalloproteins, blue copper proteins have attracted widespread interest due to their biological functions and properties.^{1,47,48,55–64} The blue copper proteins exhibit three properties that are different from the small inorganic copper complexes: a strong absorption around 600 nm, a small narrow hyperfine coupling constant, and a high-reduction potential.^{1–3,65–68} These proteins can be classified into three types on the basis of their geometrical environment around the metal site. AZ belongs to the type 1 copper site. It transports an electron from cytochrome *c*₅₅₁ to a soluble nitrite reductase (*cd*₁) in the periplasmic space of the bacterium.^{69–71} The secondary structural topology of AZ consists of a short α -helix and eight β -strands constituting two β -sheets folded into a Greek key motif.

In the active site of AZ, the copper ion is covalently bonded to the thiolate group of cysteine [S²⁻(C112)] and coordinated with nitrogen atoms of two histidine residues [N^{δ1}(H46) and N^{δ1}(H117)] in a trigonal planar conformation. The thioether group of the methionine [S^δ(M121)] serves as an axial ligand, resulting in a trigonal pyramidal coordination geometry around the copper ion. A second axial group, the backbone amide oxygen of the glycine [O(G45)], electrostatically interacts with the copper ion, resulting in distorted trigonal bipyramidal (TBP) geometry around the metal ion coordination site.^{1–3,65–68}

Furthermore, the copper center lying at one end of this architecture is shielded from the solvent by the loop that links the two C-terminal strands.^{72–76} This loop contains the coordinating cysteine [S²⁻(C112)], histidine [N^{δ1}(H117)], and axial methionine [S^δ(M121)] residues. The analysis of different cupredoxins reveals that the length, sequence, and composition of loops are different for different systems.^{72–76} Thus, it is possible to modify the copper environment and tune important properties by manipulating this loop without compromising the metal binding. Dennison and co-workers have made significant contributions to the loop-directed mutagenesis of AZ.^{72–76} The loop present in the native AZ has been replaced by that of plastocyanin (PC) and amicyanin (AMI). These loop-contracted AZ are designated as AZPC⁷⁴ (the loop of AZ is replaced by that of PC), AZAMI⁷³ (the loop of AZ is replaced by that of AMI), and AZAMI-F⁷³ (the AZ loop is replaced by the AMI loop without a F residue). Both native and loop-mutated AZs are shown in Figure 1.

An intricate hydrogen-bonding (H-bonding) network exists around the copper center of AZ, which stabilizes the structure of the active site.^{1,7,47,72} In the native and metal ion-substituted AZs, the thiolate sulfur of the S²⁻(C112) ligand accepts two H-bonds from the backbone nitrogen of asparagine (N47) and phenylalanine (F114). In AZPC, AZAMI, and AZAMI-F, the

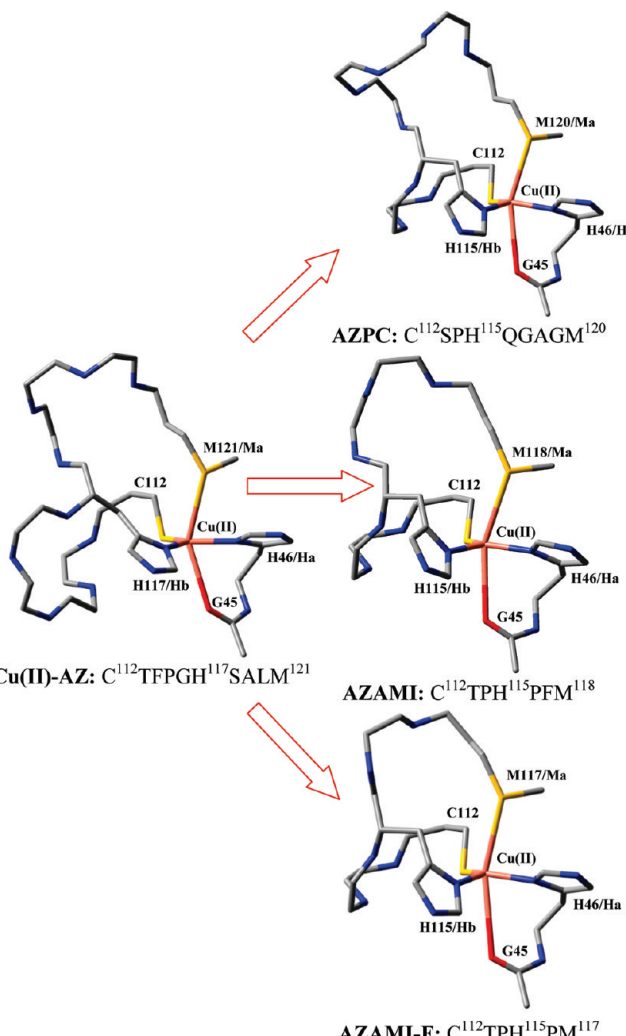


Figure 1. Active site structure of native Cu(II)-AZ (4AZU) and loop-contracted AZPC (2HX7),⁷⁴ AZAMI (2FTA),⁷³ and AZAMI-F (2FT6).⁷³ The arrows indicate the engineered AZs resulting from loop mutagenesis: AZPC (with loop sequence C¹¹²SPH¹¹⁵QGAGM¹²⁰), AZAMI (with loop sequence C¹¹²TPH¹¹⁵PFM¹¹⁸), and AZAMI-F (with loop sequence C¹¹²TPH¹¹⁵PM¹¹⁷). Equatorial ligands of H46, H115, and H117 are represented as Ha and Hb, respectively. The axial ligands of M117, M118, M120, and M121 are represented as Ma.

second H-bond is absent due to a proline (P) residue found in the position corresponding to F114.^{73,74} Thus, the presence of a single H-bond enhances the electron density on the thiolate sulfur(C112). In addition, the absence of this H-bond to the S²⁻(C112) ligand increases the spin density on the axial S^δ(M121) ligand, and it influences the spectral and redox properties of all of the systems.⁷²

Several groups have investigated the structure–function relationship of blue copper proteins using various experimental and theoretical methods.^{24–38,42–50,55–76} Solomon and co-workers have made seminal contributions to the understanding of electronic and spectral properties of PC and AZ.^{31–34} Ryde and co-workers have performed the DFT calculations on different model compounds of these copper proteins.^{35–38} It is possible to gain insights into the relation between the structure–function of blue copper proteins using these models. Rothlisberger and co-workers have carried out the Car–Parrinello molecular dynamics (CPMD) simulation combined with time-dependent density functional theory (TDDFT) calculations to predict the electronic and spectral properties of AZ.^{49,50} Recently, we have used extensible and systematic force field (ESFF) and a two-

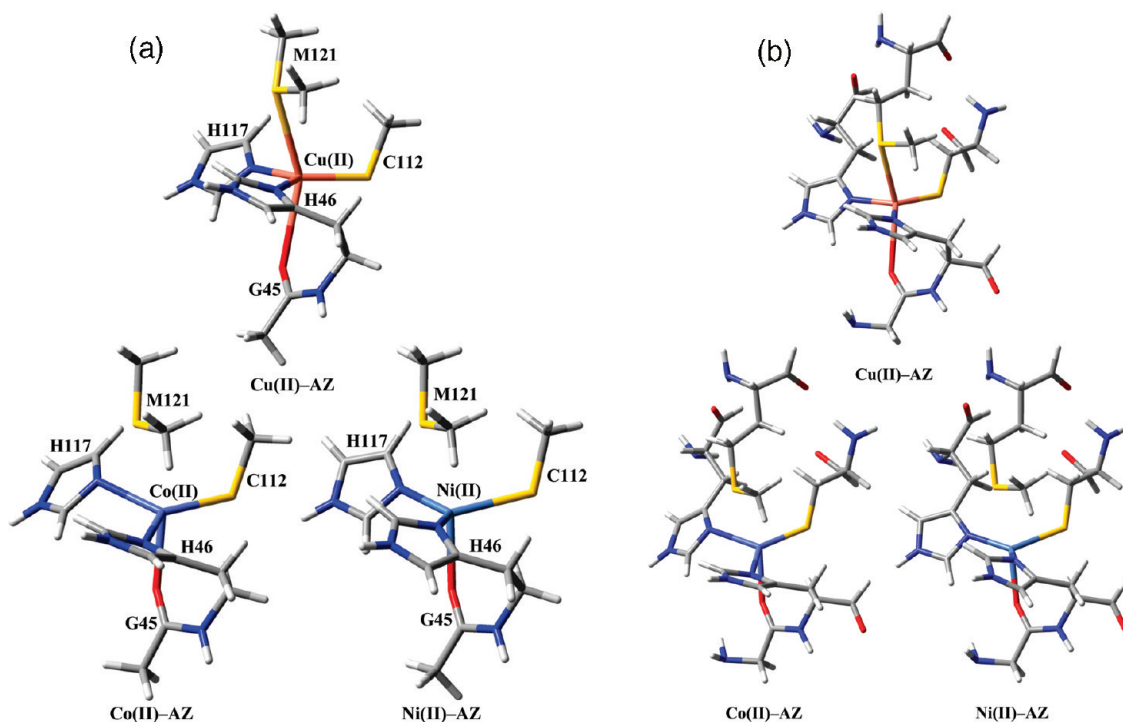


Figure 2. (a) Active site models of native and metal ion-substituted AZs. The native Cu(II)-AZ is a five-coordinated system with distorted TBP geometry. Both Co(II)- and Ni(II)-substituted AZs are four-coordinated systems with a distorted tetrahedral (T_d) geometry. (b) Cluster models of native and metal ion-substituted AZs.

layer ONIOM approach to investigate the structure and spectra of native and metal ion-substituted AZs.^{77,78}

In this study, a systematic attempt has been made to develop FF parameters for the metal site of native and metal ion-substituted AZs using the DFT (B3LYP)^{79–82} method. The new FF parameters are validated by performing MD simulations on native, loop-contracted, and metal ion-substituted AZs in combination with AMBER FF parameters for the remaining part of the protein.

2. Computational Details

The energy expression for the harmonic FF is given in eq 1:

$$E_{\text{total}} = \sum_{\text{bonds}} K_r(r - r_{\text{eq}})^2 + \sum_{\text{angles}} K_\theta(\theta - \theta_{\text{eq}})^2 + \sum_{\text{dihedrals}} \frac{V_n}{2} [1 + \cos(n\phi - \gamma)] + \sum_{i < j} \left(\frac{A_{ij}}{R_{ij}^{12}} - \frac{B_{ij}}{R_{ij}^6} + \frac{q_i q_j}{\epsilon R_{ij}} \right) \quad (1)$$

where the first and second terms are related to bond stretching and angle bending, respectively. The symbols of r , r_{eq} , and K_r are bond length, equilibrium value, and the force constant for bond stretching terms; θ , θ_{eq} , and K_θ are bond angle, equilibrium value, and the force constant for the angle bending terms, respectively. The third term corresponds to the torsional energy contributions, and φ , V_n , n , and γ are the torsion angle, periodicity, and phase angle, respectively. The last term describes nonbonded interactions.

2.1. FF Derivation From PES. The experimental crystal structures of Cu(II)-AZ, Co(II)-AZ, and Ni(II)-AZ from *Pseudomonas aeruginosa* (4AZU, 1VLX, and 1NZR) were downloaded from Brookhaven protein databank (PDB).^{65,83,84} The truncated active sites and the cluster models of native and metal ion-substituted AZs are shown in Figure 2a,b. The

hydrogen atoms were added to the models, and their positions were optimized at the B3LYP/6-31G(d,p)⁸⁵ level by freezing coordinates of heavy atoms. The PES scans were performed using the DFT (B3LYP) method employing the 6-31G(d,p) basis set to predict the stretching and bending force constants for the truncated active site models of native and metal ion-substituted AZs. The PES scans were carried out by a systematic variation of the $M(\text{II})-\text{L}$ distances and ligand–metal ion–ligand [$\text{L}-M(\text{II})-\text{L}$] angles by fixing all other coordinates. All calculations were carried out using Gaussian 03 (Revision E.01) package.⁸⁶ The potential energy barriers for the dihedral angles centered on a metal ion are usually considered to be of minor importance for the dynamics and energetics of metalloproteins.³⁵ Therefore, all force constants for dihedral angles with a metal ion as the second or third atom were set to zero.

2.2. Calculation of Partial Charges. Atomic charges for the metal ions and all of the other atoms in the cluster models were calculated using the B3LYP/6-31G(d,p) level of theory.^{66,79–84} The van der Waals (R) parameters for copper, cobalt, and nickel were taken as 1.17, 2.00, and 1.63 Å, respectively,^{24,87,88} and ϵ was taken as 0.05 kcal/mol.²⁴ The restrained electrostatic potential (RESP) charges were generated by the standard method prescribed in the AMBER package.⁸⁹ RESP partial charges for various systems are presented in the Supporting Information (Tables S1–S3).

2.3. Protocol for MD Simulation. The initial coordinates of AZ were downloaded from the X-ray crystal structure of AZ (4AZU⁶⁵) with Cu(II) ion, AZPC (2HX7⁷⁴), AZAMI (2FTA⁷³), and AZAMI-F (2FT6⁷³). Hydrogen atoms were added (using LEaP program) to the protein to mimic the structure at physiological pH. The charges of amino acids were treated appropriately using AMBER parameters. The charges of glutamate and aspartate residues were assigned as -1 , while those of lysine and arginine residues were set as $+1$, and all N^{+2} -positions of histidines were protonated. The deprotonated model of C112 residue was used in all of these calculations.

The MD simulations were carried out using the AMBER 10 package employing ff03 FF parameters.^{89,90} All MD simulations were performed by applying periodic boundary conditions (PBC) and also in an explicit solvent (TIP3P water molecules)⁹¹ environment. The native and metal ion-substituted AZs were solvated with 6934 water molecules, and the truncated octahedral box was used for the calculation (initial volume 260539.8 Å³). For the loop-contracted AZ models, the numbers of water molecules included in the calculations were 6470, 6796, and 6122. The initial volumes of the boxes were 245308.4, 254323.5, and 233313.1 Å³ for AZPC, AZAMI, and AZAMI-F systems, respectively. The isothermal–isobaric (NPT) ensemble was employed with PBC. The particle mesh Ewald (PME) summation was used to treat long-range electrostatic interactions, while a typical 12 Å cutoff was used for the van der Waals interactions.⁹² The constant pressure (1 atm) was maintained using Berendsen weak-coupling algorithm with a relaxation time constant of 2 ps.⁹³ The temperature of the system was maintained at 300 K using a Langevin thermostat with a time constant for heat bath coupling of 1 ps.⁹⁴ The bond length involving hydrogen atoms was constrained using the SHAKE algorithm with a relative geometric tolerance of 0.0001.⁹⁵ To validate the new set of FF parameters, MD simulations on native [Cu(II)–AZ], loop-contracted (AZPC, AZAMI, and AZAMI-F), and metal ion-substituted AZs [Co(II)–AZ and Ni(II)–AZ] models were carried out. The equilibration of the system was evaluated by monitoring the fluctuations in the potential energy, kinetic energy, and temperature with time. In addition, the variation of root mean square deviation (rmsd) with time was also monitored to ensure the equilibration. Equilibration was performed for 2 ns. After equilibration, the production run was carried out for 10 ns. The trajectories were saved for every 1 ps interval for further analysis. The postprocessing of the trajectories was carried out using the PTRAJ package. The various parameters obtained from the MD trajectories are defined in the following section.

3. Definition of Various Parameters

3.1. Root Mean Square Deviation (rmsd). The backbone (C–C^α–N) and C^α-atom rmsd were calculated with respect to the initial conformation as a function of time using eq 2.

$$\text{rmsd}(t) = \left[\frac{1}{N} \sum_{i=1}^N \left\| \mathbf{r}_i(t) - \mathbf{r}_i(0) \right\|^2 \right]^{1/2} \quad (2)$$

where $r_i(t) - r_i(0)$ is the difference between instantaneous and starting position of the same atom. N is the total number of backbone and C^α atoms.

3.2. Radius of Gyration (R_g). The R_g is especially useful to measure the compactness of a structure. The R_g is defined as the root mean square distance of the collection of atoms from their common center of mass. The R_g of a system can be calculated using eq 3.

$$R_g = \sqrt{\frac{\sum_i m_i r_i^2}{\sum_i m_i}}^{1/2} \quad (3)$$

where m_i is the mass of atom i and r_i is the position of atom i with respect to the center of mass of the molecule. The R_g was computed for all C^α atoms present in the protein.

3.3. Atomic Fluctuation Analysis. The atomic fluctuations can be estimated from the B factor by using eq 4:

$$B_i = \frac{8\pi^2}{3} \langle \Delta r_i \rangle^2 \quad (4)$$

where Δr_i is the root mean square positional fluctuation of atom i . The simulated B factors were calculated using the time-averaged coordinates obtained from 10 ns of simulation.

3.4. H-Bonding Analysis. The H-bonding parameters were obtained from the trajectory using the geometrical criteria as given in eq 5.

$$H_i = \begin{cases} 1, [d(\text{donor atom}_i \cdots \text{acceptor atom}_i) 3.5 \text{ \AA}] \text{ and} \\ [120^\circ \leq \text{angle(donor atom}_i \cdots \text{H-acceptor atom}_i) \leq 180^\circ] \\ 0, \text{ otherwise} \end{cases} \quad (5)$$

where H_i is the possible i -th inter- and intramolecular hydrogen bond pattern in the system. The occupancy of the H-bonds was determined according to the expression in eq 6.

occupancy of H-bond in % =

$$\left[\frac{\text{total no. of } H_i = 1 \text{ state}}{\text{total no. of conformations}} \right] \times 100 \quad (6)$$

3.5. Dynamic Cross-Correlation Matrices (DCCM) Analysis. The DCCM describes the coordinated fluctuations of the atomic positions of C^α atoms from their average values obtained from 10 ns of the simulations. For the displacement vectors Δr_i and Δr_j of atoms i and j , the matrix C_{ij} is defined in eq 7:

$$C_{ij} = \frac{\langle \Delta r_i \cdot \Delta r_j \rangle}{\sqrt{\langle \Delta r_i^2 \rangle} \sqrt{\langle \Delta r_j^2 \rangle}} \quad (7)$$

where i and j may be any two atoms, residues, or domains, Δr_i and Δr_j are the displacement from the average position of an amino acid. If $C_{ij} = 1$, the fluctuations of i and j are in complete correlation (same period and same phase); if $C_{ij} = -1$, the fluctuations of i and j are completely anticorrelated (same period and opposite phase); and if $C_{ij} = 0$, the fluctuations of i and j are not correlated. DCCM analysis was carried out for all of the model systems.

4. Results and Discussion

4.1. Derivation of FF Parameter From PES. The rigid body PES calculated at the DFT (B3LYP/6-31G(d,p)) level for Cu(II)–L distances and L–Cu(II)–L angles for the metal site of Cu(II)–AZ are given in Figures 3 and 4. The parameters obtained from the fit of rigid body PESs of M(II)–L and L–M(II)–L [where M(II) = Cu(II), Co(II), and Ni(II)] are listed in Tables 1–3. The PESs of other metal ion-substituted AZs are presented in the Supporting Information (Figures S1–S4). The calculated Cu(II)–S'(C112), Cu(II)–N^{δ1}(H46), Cu(II)–N^{δ1}(H117), Cu(II)–S^δ(M121), and Cu(II)–O(G45) distances are 2.148, 1.965, 1.936, 3.430, and 2.760 Å, respectively. The X-ray diffraction values for these distances are 2.237 ± 0.044, 2.076 ± 0.060, 2.011 ± 0.069, 3.149 ± 0.070, and 2.967 ± 0.093 Å, respectively.⁶⁵ The calculated M(II)–L

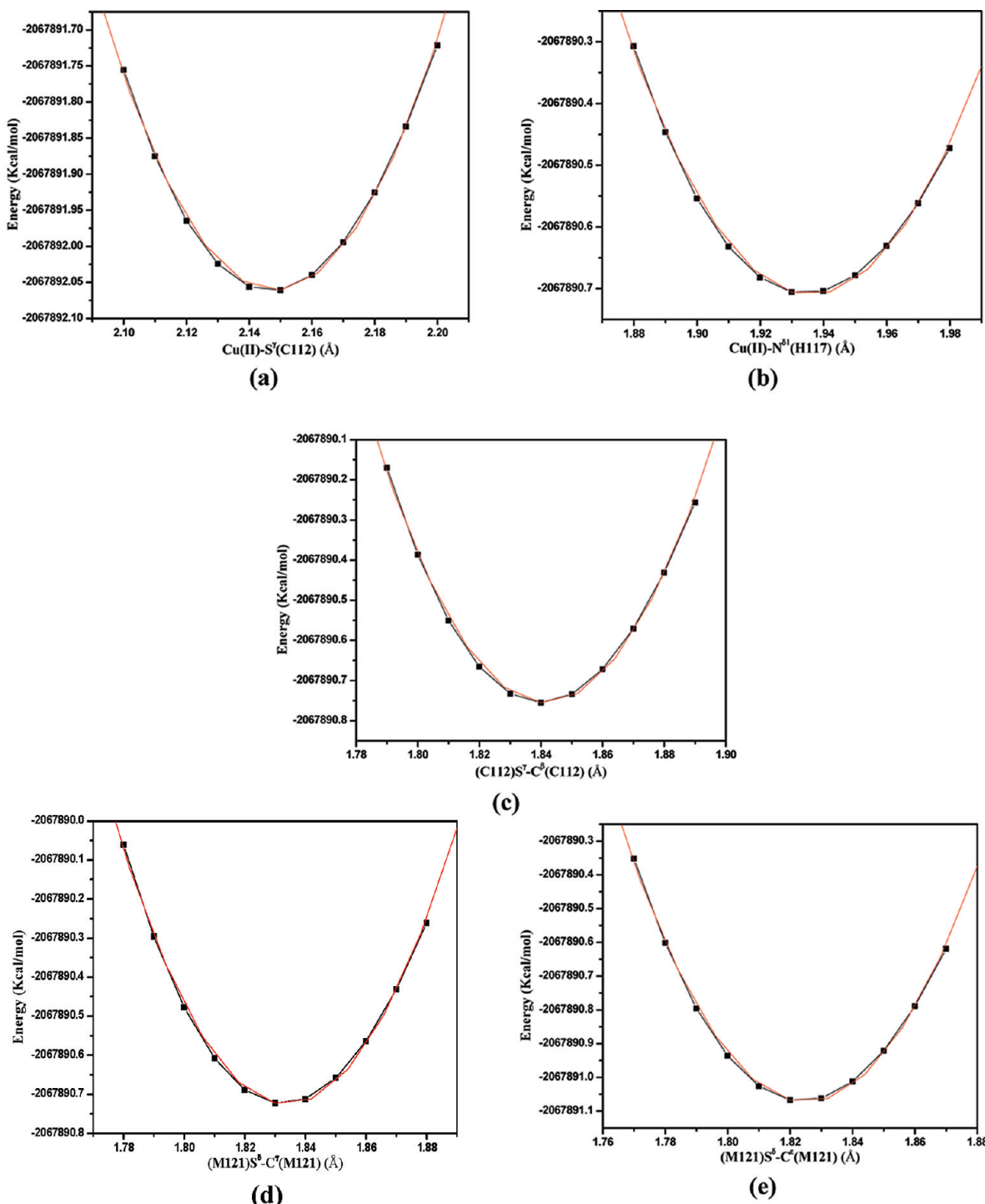


Figure 3. Calculated and fitted PES for metal ligand distances: (a) Cu(II)-S^γ(C112), (b) Cu(II)-N^{δ1}(H117), (c) (C112)S^γ-C^β(C112), (d) (M121)S^δ-C^γ(M121), and (e) (M121)S^δ-C^ε(M121).

distances are in reasonable agreement with that of X-ray diffraction values. A similar agreement has also been found in the case of bond angles involving L-M(II)-L. It is well-known that calculated geometrical parameters depend on the level of electronic structure calculation and the quality of the basis set. Thus, the discrepancies between the calculated geometrical parameters and the X-ray diffraction values can be attributed to the above-mentioned factors.

The calculated equatorial ligand Cu(II)-S^γ(C112), Cu(II)-N^{δ1}(H46), and Cu(II)-N^{δ1}(H117) force constants are around 129, 108, and 126 kcal/mol Å², respectively, and the axial ligand Cu(II)-S^δ(M121) and Cu(II)-O(G45) force con-

stants are around 4 and 6 kcal/mol Å² for the native AZ. It can be noted that axial ligand force constants are considerably smaller than those of equatorial ligands. These results are in good agreement with the previous experimental and theoretical values.^{47,96,97}

4.2. Validation of FF Parameter. 4.2.1. MD Simulation for Native and Loop-Contracted AZs. From the MD trajectories of native and loop-contracted AZs, the time evolution of structural properties and energies has been obtained. The calculated rmsd values are listed in Table 4. The rmsd between native and loop-contracted systems are shown in Figure 5a. The plot of R_g with time for all systems is presented in Figure 6a.

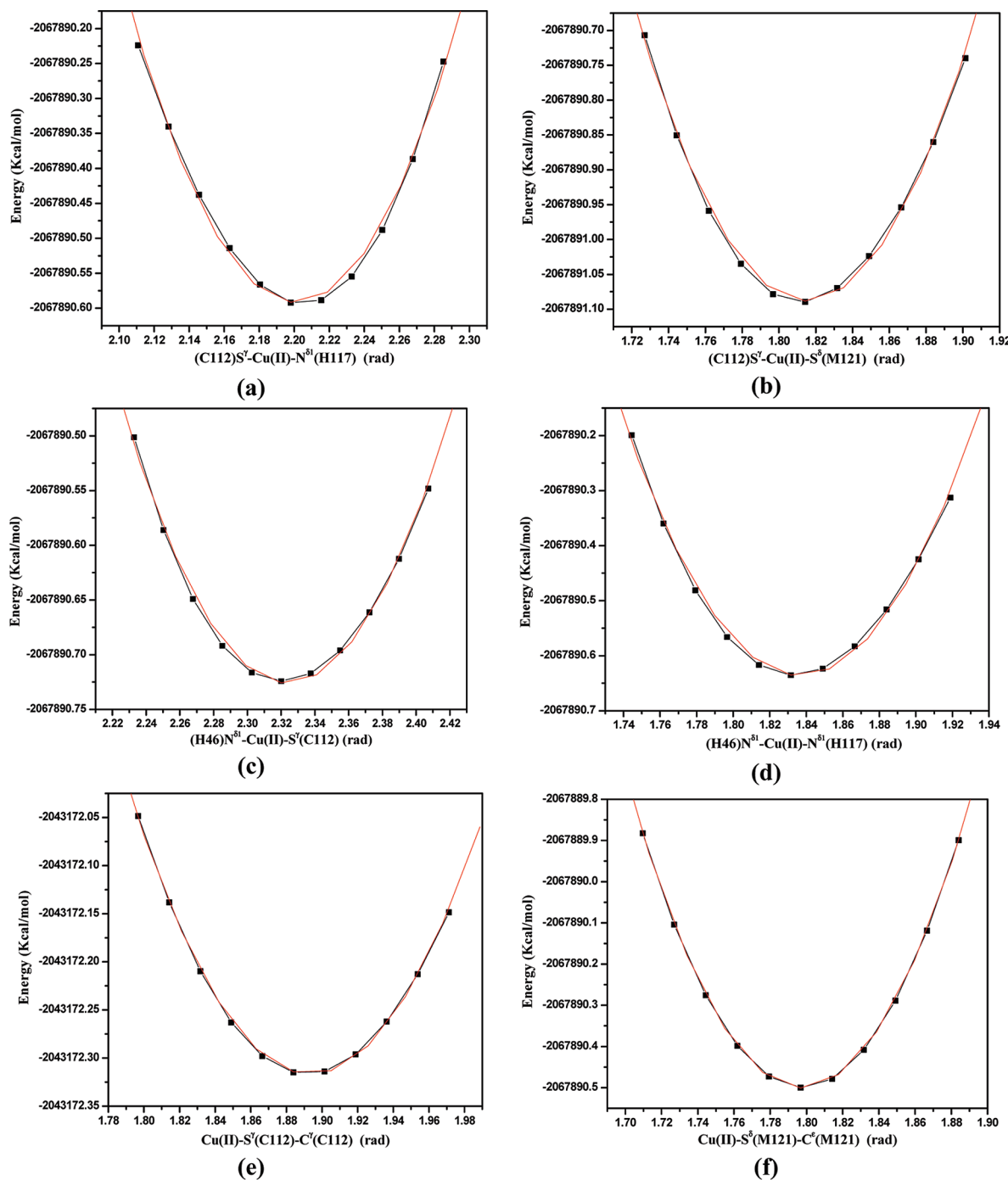


Figure 4. Calculated and fitted PES for metal-centered angles: (a) $(\text{C}112)\text{S}^\gamma-\text{Cu}(\text{II})-\text{N}^{\delta 1}(\text{H}117)$, (b) $(\text{C}112)\text{S}^\gamma-\text{Cu}(\text{II})-\text{S}^\delta(\text{M}121)$, (c) $(\text{H}46)\text{N}^{\delta 1}-\text{Cu}(\text{II})-\text{S}^\gamma(\text{C}112)$, (d) $(\text{H}46)\text{N}^{\delta 1}-\text{Cu}(\text{II})-\text{N}^{\delta 1}(\text{H}117)$, (e) $\text{Cu}(\text{II})-\text{S}^\gamma(\text{C}112)-\text{C}^\beta(\text{C}112)$, and (f) $\text{Cu}(\text{II})-\text{S}^\delta(\text{M}121)-\text{C}^\epsilon(\text{M}121)$.

The R_g varies from 13.5 to 14.0 Å for Cu(II)-AZ, AZPC, AZAMI, and AZAMI-F. The average B factor values for the native and loop-contracted AZs are given in Table 5. All of these results show that there are no significant changes in the overall structure, conformation of individual secondary structural elements, and the complete topology of loop-contracted AZs when compared with the native protein. These findings are in good agreement with the previous experimental studies on the same systems.^{65,73,74}

4.2.2. Geometrical Parameters of Native and Loop-Contracted AZs. The calculated geometrical parameters for the native, loop-contracted, and metal ion-substituted AZs are presented in Tables 6 and 7 along with values reported in the previous experimental and computational studies. It can be

seen from Table 6 that the calculated $\text{M}(\text{II})-\text{S}^\gamma(\text{C}112)$, $\text{M}(\text{II})-\text{N}^{\delta 1}(\text{H}46)$, $\text{M}(\text{II})-\text{N}^{\delta 1}(\text{H}117)$, $\text{M}(\text{II})-\text{S}^\delta(\text{M}121)$, and $\text{M}(\text{II})-\text{O}(\text{G}45)$ distances in this investigation are in good agreement with those values obtained from the X-ray diffraction structure and previously predicted values.^{47,65,73,74} The axial ligand distances corresponding to M121 and G45 residues are 3.513 (0.183) and 2.863 (0.171) Å for Cu(II)-AZ.^{45,65} The corresponding distances from the X-ray diffraction study are 3.149 ± 0.070 and 2.967 ± 0.093 Å, respectively.⁴⁷ It can be observed that the deviations in $\text{M}(\text{II})-\text{L}$ distances are within the experimental error values.⁴⁷ The active site geometries of ACPC, AZAMI, and AZAMI-F are remarkably identical to those of AZ except for lengthening of the Cu(II)-O(G45) distance, which is due to the movement of copper ion away

TABLE 1: Calculated Bond Distances, Bond Angles, and Corresponding Force Constants for the Native AZ

bond	K_r (kcal/mol Å ²)	r_{eq} (Å)
Cu(II)–S ^γ (C112)	129.0	2.148
Cu(II)–N ^{δ1} (H46)	107.7	1.965
Cu(II)–N ^{δ1} (H117)	126.4	1.936
Cu(II)–S ^δ (M121)	3.6	3.430
Cu(II)–O(G45)	5.6	2.760
(C112)S ^γ –C ^β (C112)	216.8	1.841
(M121)S ^δ –C ^γ (M121)	224.9	1.834
(M121)S ^δ –C ^ε (M121)	232.7	1.825
angle	K_θ (kcal/mol rad ²)	θ_{eq} (deg)
(C112)S ^γ –Cu(II)–N ^{δ1} (H117)	46.8	126.2
(C112)S ^γ –Cu(II)–S ^δ (M121)	48.0	104.4
(H117)N ^{δ1} –Cu(II)–S ^δ (M121)	24.6	85.3
(H46)N ^{δ1} –Cu(II)–S ^γ (C112)	26.2	133.2
(H46)N ^{δ1} –Cu(II)–N ^{δ1} (H117)	49.9	105.3
(H46)N ^{δ1} –Cu(II)–S ^δ (M121)	35.0	81.1
(G45)O–Cu(II)–S ^γ (C112)	43.5	104.0
(G45)O–Cu(II)–N ^{δ1} (H117)	71.3	82.4
(G45)O–Cu(II)–S ^δ (M121)	45.1	151.6
Cu(II)–S ^γ (C112)–C ^β (C112)	28.4	108.5
Cu(II)–S ^δ (M121)–C ^ε (M121)	80.0	103.0
(M121)C ^γ –S ^δ (M121)–C ^ε (M121)	116.7	98.3

TABLE 2: Calculated Bond Distances, Bond Angles, and Corresponding Force Constants for Co(II)–AZ

bond	K_r (kcal/mol Å ²)	r_{eq} (Å)
Co(II)–S ^γ (C112)	127.8	2.193
Co(II)–N ^{δ1} (H46)	76.5	2.095
Co(II)–N ^{δ1} (H117)	88.4	2.056
Co(II)–O(G45)	28.4	2.178
(C112)S ^γ –C ^β (C112)	219.1	1.842
angle	K_θ (kcal/mol rad ²)	θ_{eq} (deg)
(C112)S ^γ –Co(II)–N ^{δ1} (H117)	33.4	126.3
(H46)N ^{δ1} –Co(II)–S ^γ (C112)	37.8	134.4
(H46)N ^{δ1} –Co(II)–N ^{δ1} (H117)	27.0	107.0
(G45)O–Co(II)–S ^γ (C112)	43.0	105.8
(G45)O–Co(II)–N ^{δ1} (H117)	35.7	92.4
Co(II)–S ^γ (C112)–C ^β (C112)	32.3	107.2

TABLE 3: Calculated Bond Distances, Bond Angles, and Corresponding Force Constants for Ni(II)–AZ

bond	K_r (kcal/mol Å ²)	r_{eq} (Å)
Ni(II)–S ^γ (C112)	110.9	2.211
Ni(II)–N ^{δ1} (H46)	80.4	2.038
Ni(II)–N ^{δ1} (H117)	120.4	1.966
Ni(II)–O(G45)	57.5	2.008
(C112)S ^γ –C ^β (C112)	225.9	1.834
angle	K_θ (kcal/mol rad ²)	θ_{eq} (deg)
(C112)S ^γ –Ni(II)–N ^{δ1} (H117)	15.4	108.0
(H46)N ^{δ1} –Ni(II)–S ^γ (C112)	20.0	109.0
(H46)N ^{δ1} –Ni(II)–N ^{δ1} (H117)	27.5	114.3
(G45)O–Ni(II)–S ^γ (C112)	30.5	104.6
(G45)O–Ni(II)–N ^{δ1} (H117)	59.2	95.9
Ni(II)–S ^γ (C112)–C ^β (C112)	31.3	106.8

from this residue.^{73,74} Similarly, the M(II)–S^δ(M121) bond distance becomes slightly larger than that of native AZ. This may be due to the inherent PES and floppy nature of these axial ligands. Consequently, the copper atom is further displaced from the plane of the three equatorial ligands.^{73,74} It is evident from Table 7 that the calculated L–M(II)–L angles are in reasonable agreement with X-ray structure and other values reported in earlier studies. A systematic comparison of bond angles obtained from the FF calculation with the X-ray diffraction values reveals

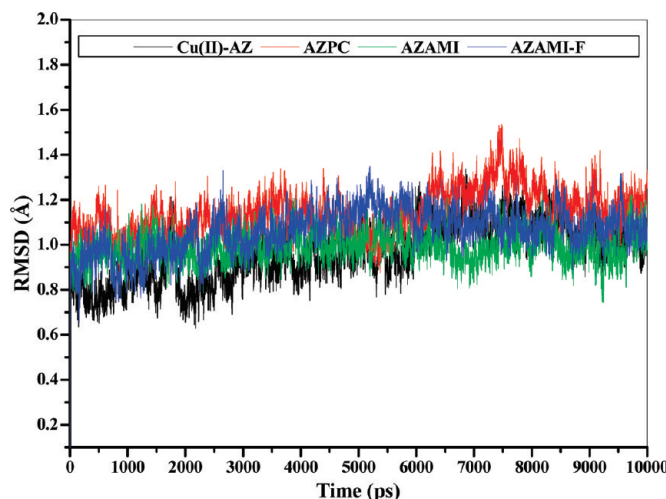
TABLE 4: Calculated Average rmsd Between the Crystal and the MD Structures of Cu(II)–AZ, AZPC, AZAMI, AZAMI-F, Co(II)–AZ, and Ni(II)–AZ (Å)

AZ	backbone atoms		C ^a -atom	
	mean	SD	mean	SD
Cu(II)–AZ	0.97	0.13	1.00	0.13
AZPC	1.14	0.10	1.16	0.10
AZAMI	0.99	0.06	1.01	0.07
AZAMI-F	1.06	0.10	1.08	0.10
Co(II)–AZ	1.13	0.11	1.15	0.12
Ni(II)–AZ	1.06	0.12	1.09	0.13

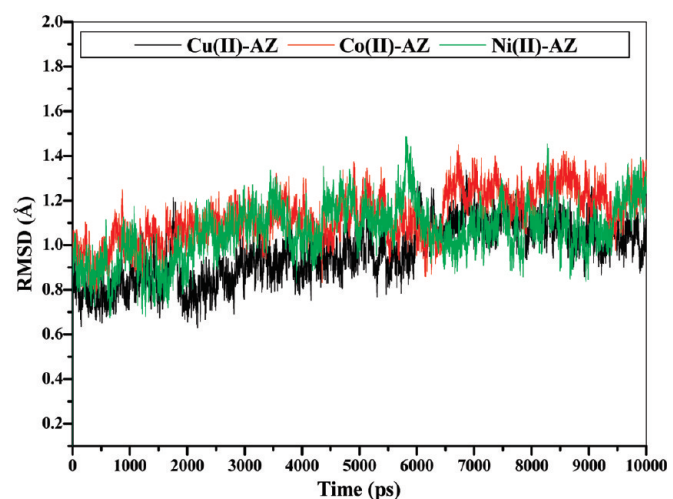
that the percentage of error in the bond angles ranges from 0.68–9.78, 0.76–10.12, 0.00–10.30, and 0.00–11.45 for Cu(II)–AZ, ACPC, AZAMI, and AZAMI-F, respectively.

4.3. MD Simulation of Metal Ion-Substituted AZs. With a view to probe the effect of metal ion-substitution, Cu(II) was substituted with metal ions such as Co(II) and Ni(II).^{1,65,83,84} The calculated rmsd values between the native and the metal ion-substituted AZs are given in Figure 5b, and the same values are summarized in Table 4. The variation of R_g with time is depicted in Figure 6b. The R_g values vary from 13.6 to 14.0 Å for Co(II)–AZ and Ni(II)–AZ. The average B factor values of metal ion-substituted AZs are listed in Table 5. All of these results elicit the structures of metal ion-substituted systems and do not undergo any drastic conformational changes when compared to that of native one.

4.3.1. Geometrical Parameters of Metal Ion-Substituted AZs. Among the different blue copper proteins, the coordination number of the AZ is five.¹ The axial (G45)O position interacts Coulombically with the Cu(II) ion, which differentiates AZ from the other blue copper proteins.⁸⁴ The calculated geometrical parameters of the metal ion-substituted AZs are presented in Tables 6 and 7. Specifically, the axial ligand distances [Cu–S^δ(M121) and Cu–O(G45)] differ considerably from that of native AZ due to the inherent shallow nature of the corresponding PESs. In the metal ion-substituted AZs, M(II)–L distances are longer except for the backbone oxygen ligand, which is shorter by ~0.6 Å. As a result, the M(II) ion moves in the direction of the G45 backbone oxygen atom. Ni(II)–AZ coordinates more strongly with the carbonyl oxygen of O(G45) as a result Ni(II)–S^δ(M121) distance increases by 3.691 Å.^{83,84} Substitution of Cu(II) by Co(II) and Ni(II) leads to a loss of covalency of the M(II)–S^δ(M121) bond, and as a consequence, the electrostatic interaction between the metal ion and the O(G45) increases. The calculated L–M(II)–L angles are in reasonable agreement with the X-ray and other values observed in the previous studies.^{47,77,78,83,84} The comparison of bond angles obtained from MD simulations with the X-ray diffraction values show that the percentage of error in the bond angle ranges from 0.00 to 14.02 and 1.68 to 11.11 for Co(II)–AZ and Ni(II)–AZ, respectively. Although the overall structures of metal ion-substituted AZs do not undergo any significant changes, the distorted TBP geometry of the active site of native Cu(II)–AZ varies to distorted tetrahedral (T_d) arrangement upon substitutions with other metal ions.^{65,83,84,98–100} There are no other significant changes in the overall conformation of the metal ion-substituted AZs. It is interesting to note that the geometrical parameters obtained from the present investigation are closer to the values of those predicted from the previous studies and deviations in M(II)–L distances and L–M(II)–L angles are within the experimental error.^{47,83,84} These results clearly reinforce that the new set of FF parameters can be used to predict the active site geometry of the native and metal ion-substituted AZs.



(a) RMSD Between Native and Loop-Contracted AZs



(b) RMSD Between Native and Metal Ion-Substituted AZs

Figure 5. Variation of rmsd of backbone of native, loop-contracted, and metal ion-substituted AZs with respect to their initial structure.

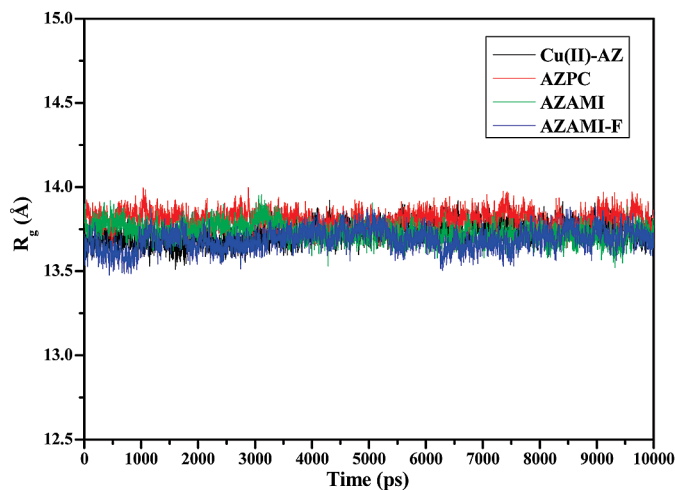
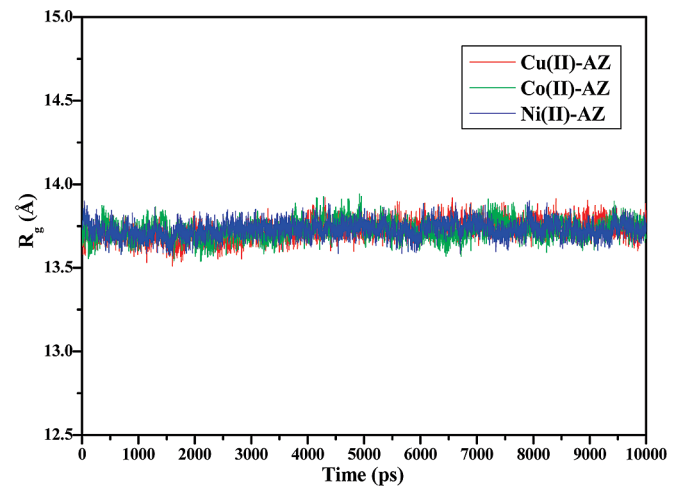
(a) R_g Between Native and Loop-Contracted AZs(b) R_g Between Native and Metal Ion-Substituted AZs

Figure 6. Radius of gyration (R_g) of native, loop-contracted, and metal ion-substituted AZs for the entire protein structure.

TABLE 5: Calculated Average B Factor for Cu(II)-AZ, AZPC, AZAMI, AZAMI-F, Co(II)-AZ, and Ni(II)-AZ (\AA^2)

AZ	backbone atoms		C^α -atom	
	mean	SD	mean	SD
Cu(II)-AZ	5.29	0.30	5.29	0.31
AZPC	5.74	1.54	5.75	1.56
AZAMI	4.74	1.22	4.76	1.23
AZAMI-F	6.11	2.29	6.12	2.30
Co(II)-AZ	5.52	0.93	5.53	0.94
Ni(II)-AZ	3.86	0.96	3.88	0.97

4.4. H-Bond Analysis of Native, Loop-Contracted, and Metal Ion-Substituted AZs. As mentioned in the earlier section, an intricate H-bond network is observed in the native AZ. Variations in the different H-bonds that are observed in the immediate vicinity of the metal site have been calculated from the MD trajectories for all of the systems. The calculated H-bond parameters are presented in the Supporting Information (Tables S4–S7). In the case of Cu(II)-AZ, the N-terminal histidine ligand, $N^{e2}(H46)$, $O(H46)$, and $N(H46)$ form H-bonds with the $O(N10)$, tyrosine [$N(Y87)$ and $O(Y87)$], respectively. The backbone amide nitrogen [$N(N47)$], side chain $O^{\delta 1}(N47)$, and $N^{\delta 2}(N47)$ make H-bonds with $S^{\gamma}(C112)$, threonine [$N(T113)$ and $O^{\gamma 1}(T113)$], respectively. In addition, the backbone nitrogen

of F114 is H-bonded to $S^{\gamma}(C112)$ with a $(C112)S^{\gamma}\cdots N(F114)$ distance of 3.552 Å.

The native AZ consists of other important H-bonds involving the metal sites. They are (i) connecting the backbone nitrogen of C112 and the backbone oxygen of M121 at 3.011 Å, (ii) involving the backbone nitrogen of M121 and the backbone oxygen of H117 at 2.815 Å, and (iii) the backbone nitrogen of H117 and the backbone oxygen of F114 at 2.985 Å. In AZ, the thiolate sulfur of the C112 ligand accepts two H-bonds from the backbone nitrogen of N47 and F114. Furthermore, the loop of AZ contains intraloop (C112–F114/M121, H117–F114/P115/L120/M121, A119–K122, and L120–K112) H-bonds. The results presented in the Supporting Information (Tables S4) reveal that the fluctuations in these H-bonding interactions are within the criteria defined for the H-bonding distance and angle. The calculated H-bond distances are in reasonable agreement with those obtained from X-ray diffraction.⁶⁵

It can be seen from the Supporting Information (Tables S4–S7) that the geometrical parameters of H-bonding interactions patterns (S.No.1–6) are similar to all the systems. In the case of AZPC model, residues in the loop participate in both intra- and inter-H-bonding. Because the H-bonding in the nearby coordination environment of the metal site is significantly

TABLE 6: Calculated Average Bond Distances of the Native, Loop-Contracted, and Metal Ion-Substituted AZs (Å)

	M(II)–N ^{δ1} (Ha ^g)	M(II)–S ^γ (C112)	M(II)–N ^{δ1} (Hb ^g)	M(II)–O(G45)	M(II)–S ^δ (Ma ^g)
native AZ					
X-ray structure of Cu(II)–AZ ^a	2.076 ± 0.060	2.237 ± 0.044	2.011 ± 0.069	2.967 ± 0.093	3.149 ± 0.070
Solomon et al. ^b	2.06	2.21	2.03	2.68	3.06
Swart et al. ^a	2.017	2.169	1.995	2.855	3.178
Rothilsberger et al. ^c	1.980 ± 0.060	2.130 ± 0.040	1.990 ± 0.050	3.200 ± 0.220	3.320 ± 0.280
ESFF ^d	2.06	2.36	2.05	2.92	3.16
ONIOM ^d	1.956	2.140	1.945	2.947	3.356
Hillier et al. (ONIOM EE) ^e	1.99	2.17	2.01	2.55	3.53
Cu(II)–AZ present study ^f	1.969 (0.052)	2.164 (0.047)	1.936 (0.048)	2.863 (0.171)	3.513 (0.183)
loop-contracted AZs					
X-ray structure of AZPC ^h	2.048	2.205	2.084	3.195	3.103
AZPC present study ^f	1.958 (0.051)	2.161 (0.046)	1.942 (0.048)	2.953 (0.171)	3.591 (0.190)
X-ray structure of AZAMI ^h	1.980	2.140	2.090	3.190	3.290
AZAMI present study ^f	1.962 (0.052)	2.162 (0.047)	1.943 (0.048)	2.989 (0.180)	3.562 (0.174)
X-ray structure of AZAMI-F ^h	2.076	2.154	2.036	3.301	3.143
AZAMI-F present study ^f	1.956 (0.052)	2.161 (0.047)	1.952 (0.048)	2.981 (0.196)	3.626 (0.175)
metal ion-substituted AZs					
X-ray structure of Co(II)–AZ ^a	2.243 ± 0.045	2.337 ± 0.024	2.421 ± 0.099	2.230 ± 0.077	3.561 ± 0.126
Swart et al. ^a	2.038	2.196	2.013	2.089	3.552
ONIOM ^d	2.075	2.239	2.035	2.074	3.631
Co(II)–AZ present study ^f	2.099 (0.061)	2.222 (0.048)	2.054 (0.058)	2.308 (0.096)	3.777 (0.287)
X-ray structure of Ni(II)–AZ ^a	2.230 ± 0.090	2.390 ± 0.070	2.220 ± 0.120	2.460 ± 0.060	3.300 ± 0.050
Swart et al. ^a	2.059	2.172	2.055	2.123	3.209
ONIOM ^d	2.032	2.228	2.011	2.058	3.707
Ni(II)–AZ present study ^f	2.100 (0.060)	2.247 (0.051)	2.053 (0.050)	2.243 (0.070)	3.691 (0.314)

^a Hybrid QM/MM calculations; taken from ref 47. ^b The active site of the AZ was optimized, keeping the backbone C and N atom coordinates constrained to their crystallographic positions; taken from ref 34. ^c Hybrid QM/MM calculations; taken from ref 50. ^d Our previous studies; taken from refs 77 and 78. ^e The ONIOM calculation with electronic embedding (EE); taken from ref 100. ^f The calculated standard deviation (SD) values are given in parentheses. ^g See the subscript in Figure 1 for definition. ^h The X-ray structure of loop-contracted and metal ion-substituted AZs; taken from refs 73 and 74.

TABLE 7: Calculated Average Bond Angles for the Native, Loop-Contracted, and Metal Ion-Substituted AZs (deg)

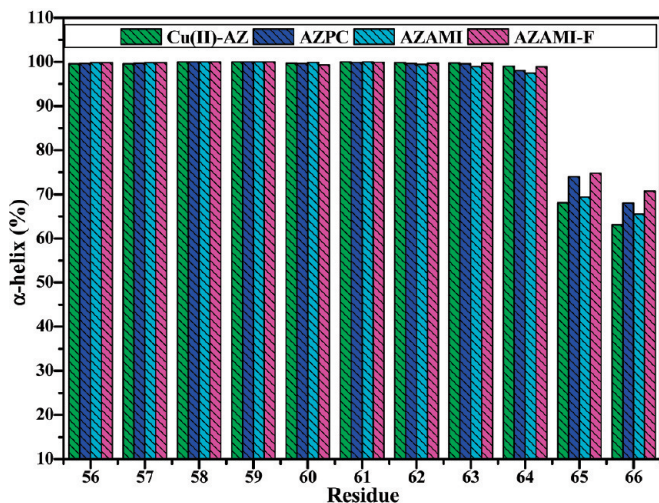
	S ^γ (C112)–N ^{δ1} (Ha) ^c –S ^γ (C112)–N ^{δ1} (Ha) ^c –S ^γ (C112)–N ^{δ1} (Hb) ^c –N ^{δ1} (Ha) ^c –S ^γ (C112)–N ^{δ1} (Hb) ^c –S ^δ (Ma) ^c –	M(II)–N ^{δ1} (Ha) ^c	M(II)–N ^{δ1} (Hb) ^c	M(II)–N ^{δ1} (Hb) ^c	M(II)–O(G45)	M(II)–O(G45)	M(II)–O(G45)	M(II)–S ^δ (Ma) ^c	M(II)–S ^δ (Ma) ^c	M(II)–S ^δ (Ma) ^c	M(II)–O(G45)
native AZ											
X-ray structure of Cu(II)–AZ ^d	130	107	122	81	100	92	69	110	84	147	
Swart et al. ^a	130	102	127		94	85		111		151	
ESFF ^b	119	123	112	73	90	84	76	83	133	141	
ONIOM ^b	131	103	126	72	108	81	74	102	95	145	
Cu(II)–AZ ^e	132	105	124	77	105	83	73	106	91	146	
loop-contracted AZs											
X-ray structure of AZPC ^d	131	104	121	74	97	78	79	111	97	150	
AZPC ^e	130	105	125	77	105	83	71	106	92	145	
X-ray structure of AZAMI ^d	134	102	123	79	97	81	76	112	92	151	
AZAMI ^e	131	106	123	75	107	83	75	104	91	147	
X-ray structure of AZAMI-F ^d	132	101	123	76	96	78	81	108	95	154	
AZAMI-F ^e	129	105	126	76	107	82	77	102	91	149	
metal ion-substituted AZs											
X-ray structure of Co(II)–AZ ^d	129	107	122	73	104		107				
ONIOM	127	113	116	87	106		94				
Co(II)–AZ ^e	132	105	122	78	108		92				
X-ray structure of Ni(II)–AZ ^d	113	120	119	87	101		108				
ONIOM	130	103	125	88	104		90				
Ni(II)–AZ ^e	123	113	121	79	109		96				

^a Hybrid QM/MM calculations; taken from ref 47. ^b Our previous studies; taken from refs 77 and 78. ^c See the subscript in Figure 1 for definition. ^d The X-ray structure of native, loop-contracted, and metal ion-substituted AZs; taken from refs 65, 73, 74, 83 and 84. ^e Present study.

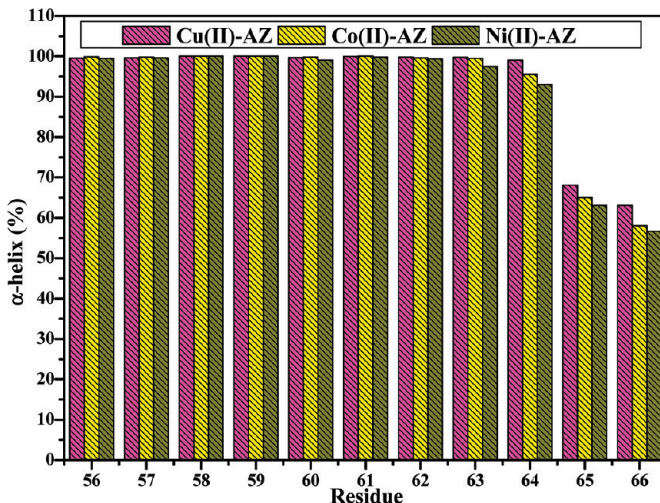
important, distances involving N47 (of backbone N atom) with S^γ(C112) were obtained from MD trajectories. The same distance for Cu–AZ, ACPC, AZAMI, and AZAMI-F models are 3.377, 3.370, 3.366, and 3.395 Å, respectively. The second H-bond involving C112 with F114 is absent in the loop-contracted models. Therefore, the loop contractions in AZ influence both the intra- and the inter-H-bonding network

patterns. These subtle structural changes are responsible for the variations in the reduction potentials of loop-contracted systems.^{72–76}

The H-bond parameters for metal ion-substituted AZs obtained from the MD simulations are listed in the Supporting Information (Tables S8 and S9). It can be seen from the results that the H-bonding network patterns observed in the metal ion-



(a) Native and Loop Contracted AZs



(b) Native and Metal Ion Substituted AZs

Figure 7. Percentage of α -helix content of the region 56–66 (a short α -helix region) for the native, loop-contracted, and metal ion-substituted AZs.

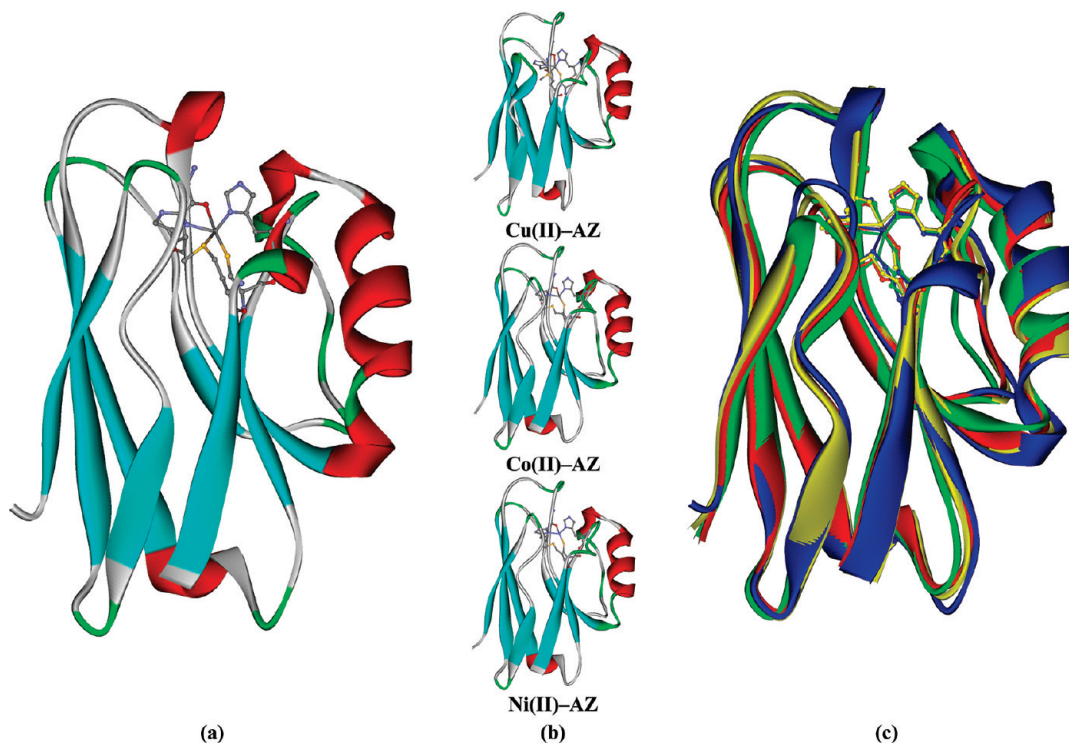


Figure 8. Ribbon representation of the structure of native and engineered AZs. (a) Crystal structure of native AZ, (b) average structures of native and metal ion-substituted AZs from MD simulation, and (c) an overlay of average structures of Cu(II)-AZ and metal ion-substituted AZs from MD simulation with native from X-ray structure (blue, red, green, and yellow colors for crystals and average structures of Cu(II)-AZ, Co(II)-AZ, and Ni(II)-AZ, respectively).

substituted models are similar to those of native AZ. The calculated values are in reasonable agreement with the X-ray diffraction results.^{72–76} However, the results given in Tables S8 and S9 in the Supporting Information reveals that the occupancy of H-bonding interactions in the metal ion-substituted AZs is different from that of native AZ due to changes in the active site geometry of metal site from distorted TBP to T_d . The comparison of the (C112)S'…N(F114) distance in various systems yields that the occupancies of this distance in Cu(II)-AZ and Co(II)-AZ are marginally less than those of Ni(II)-AZ. Similarly, the occupancies of (C112)O…O'(S118) and (L120)O…N(K122) distances of the metal ion-substituted systems are appreciably higher than those of the native system.

4.5. Analysis of Overall Structure of Various Systems. The analysis of secondary structural elements of different AZ is necessary to understand the change in overall conformation. The percentage of α -helical content in various systems obtained from 10 ns MD trajectories is shown in Figure 7. It is found that the loop mutation and metal ions substitution marginally affect the helicity of the proteins in the region 56–66. The cartoon representations of native and metal ion-substituted proteins obtained from the MD simulation are shown in Figure 8 along with the X-ray structure for the Cu(II)-AZ. These representations reveal that the metal ion-substituted systems adopt a conformation almost identical to that found in native protein. The cross-correlation coefficients obtained from DCCM analysis

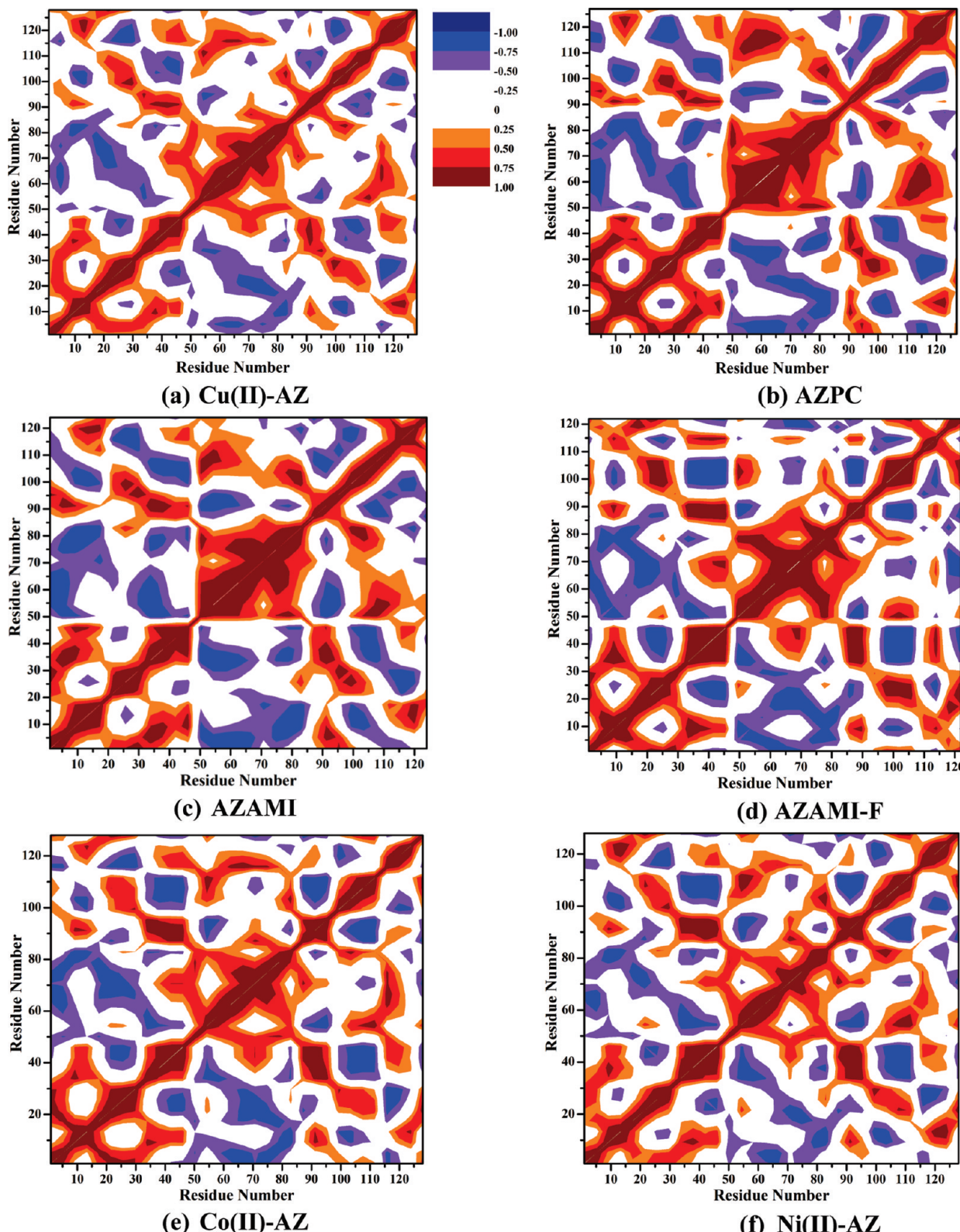


Figure 9. Calculated cross-correlation map for the C^α-atom pairs of native, loop-contracted, and metal ion-substituted AZs. Wine, red, and orange colors show the positive correlation of motions (C_{ij} is 0.50–1.0), and royal blue, blue, and violet colors show the negative correlation of motions (C_{ij} is −0.50 to −1.0).

are plotted in Figure 9. It is well-known that the strong correlated fluctuations along the diagonal occur for $i = j$, where C_{ij} is always equal to 1.00. Positive correlations originating from the diagonal indicate fluctuational correlations between contiguous residues. Off-diagonal positive and negative correlations provide information about fluctuational correlations between domains

of noncontiguous residues. These correlations include dynamical information about the C^α atoms of the entire system. It is found from the plots that there are no significant changes in the native and metal ion-substituted AZs. However, plots corresponding to the loop-mutated regions differ markedly when compared to those of the native system.

All parameters obtained from MD trajectories corresponding to Cu(II)-AZ, ACPC, AZAMI, AZAMI-F, Co(II)-AZ, and Ni(II)-AZ show that the new set of FF parameters is reliable to reproduce corresponding X-ray diffraction structures. Close scrutiny of the metal ion-substituted AZs reveals that the metal ion site undergoes significant changes from distorted TBP to distorted T_d arrangement.^{47,83,84,98,99} The overall conformation and topology of engineered systems are akin to those of the native protein.

5. Conclusions

The results obtained from this study illustrate that new FF parameters are useful to predict the structures of native and engineered copper proteins. The structures of loop-contracted AZs are almost similar to those of the native protein. Results delineate that the loop contraction does not influence the structure of the metal site of the native AZ, which is in accordance with the UV-vis spectral findings. Nevertheless, MD simulations reveal that the inherent H-bonding network of AZ is altered by the loop contraction, which in turn would influence its redox potential in agreement with the previous experimental studies. Analysis of the metal ion-substituted AZs shows that there are no considerable difference between the average structure obtained from MD simulations and the corresponding X-ray diffraction structures. However, the metal ion binding site undergoes significant changes due to the metal ion substitution. Upon metal ion substitution, the active site geometry of native AZ varies from the distorted TBP geometry to a distorted T_d arrangement, which is in accordance with the previous reports.

Acknowledgment. This study was supported by a grant from the Department of Science and Technology (DST), Government of India, New Delhi, India, under the New Initiatives in Bioinorganic Chemistry program. The authors thank Professor Ulf Ryde, Department of Theoretical Chemistry, Lund University, for providing changepot programme for RESP charge creation. Helpful suggestions from Dr. K. Sugimori, Kinjo University, Japan, are greatly appreciated. The authors thank Dr. T. Ramasami, Secretary, DST, and the Government of India for his valuable suggestions and comments and Dr. A. B. Mandal, Director, CLRI, India, for his continued support.

Supporting Information Available: Partial atomic charges and PES scan plots of native and metal ion-substituted AZs and the H-bonding parameters of the native, loop-contracted, and metal ion-substituted AZs. This material is available free of charge via the Internet at <http://pubs.acs.org>.

References and Notes

- (1) Messerschmidt, A.; Huber, R.; Poulos, T.; Wieghardt, K. *Handbook of Metalloproteins*; John Wiley & Sons: New York, 2001.
- (2) Bertini, I.; Gray, H. B.; Lippard, S. J.; Valentine, J. S. *Bioinorganic Chemistry*; Viva Publications: New Delhi, 2004.
- (3) Roat-Malone, R. M. *Bioinorganic Chemistry*; John Wiley & Sons: Hoboken, NJ, 2007.
- (4) Finkelstein, J. *Nature* **2009**, *460*, 813–813.
- (5) Waldron, K. J.; Rutherford, J. C.; Ford, D.; Robinson, N. J. *Nature* **2009**, *460*, 823–830.
- (6) Lu, Y.; Yeung, N.; Sieracki, N.; Marshall, N. M. *Nature* **2009**, *460*, 855–862.
- (7) Marshall, N. M.; Garner, D. K.; Wilson, T. D.; Gao, Y.-G.; Robinson, H.; Nilges, M. J.; Lu, Y. *Nature* **2009**, *462*, 113–116.
- (8) Zimmer, M. *Chem. Rev.* **1995**, *95*, 2629–2649.
- (9) Zimmer, M. *Coord. Chem. Rev.* **2001**, *212*, 133–163.
- (10) Zimmer, M. *Coord. Chem. Rev.* **2009**, *293*, 817–826.
- (11) Brubaker, G. R.; Johnson, D. W. *Coord. Chem. Rev.* **1984**, *53*, 1–36.
- (12) DeGrado, W. F. *Chem. Rev.* **2001**, *101*, 3025–3026.
- (13) Baltzer, L.; Nilsson, H.; Nilsson, J. *Chem. Rev.* **2001**, *101*, 3153–3164.
- (14) Jensen, F. *Introduction to Computational Chemistry*; John Wiley & Sons: New York, 1998.
- (15) Leach, A. R. *Molecular Modelling Principles and Applications*, 2nd ed.; Pearson Education Limited: England, 2001.
- (16) Comba, P.; Hambley, T. W. *Molecular Modelling of Inorganic Compounds*, 2nd ed.; Wiley VCH: Weinheim, 2000.
- (17) Cheatham, T. E., III; Case, D. A. In *Computational Studies of DNA and RNA*; Sponer, J., Lankas, F., Eds.; Springer: Dordrecht, 2006; pp 45–72.
- (18) Fuller, A. A.; Du, D.; Liu, F.; Davoren, J. E.; Bhabha, G.; Kroon, G.; Case, D. A.; Dyson, H. J.; Powers, E. T.; Wipf, P.; Gruebele, M.; Kelly, J. W. *Proc. Natl. Acad. Sci. U.S.A.* **2009**, *106*, 11067–11072.
- (19) Feldman-Sait, A.; Wade, R. C. *Molecular Recognition: Computational Analysis and Modelling*; Wiley Encyclopedia of Chemical Biology; John Wiley & Sons: New York, 2009.
- (20) Pachov, G. V.; Gabdoulline, R. R.; Wade, R. C. In *Computational Protein–Protein Interactions*; Nussinov, R., Schreiber, G., Eds.; Taylor and Francis Group LLC: Boca Raton, 2009; pp 109–128.
- (21) McCammon, J. A.; Harvey, S. C. *Dynamics of Proteins and Nucleic Acids*; Cambridge University Press: Cambridge, 1987.
- (22) Karplus, M. *Acc. Chem. Res.* **2002**, *35*, 321–323.
- (23) Simonson, T.; Archontis, G.; Karplus, M. *Acc. Chem. Res.* **2002**, *35*, 430–437.
- (24) Comba, P.; Remenyi, R. *J. Comput. Chem.* **2002**, *23*, 697–705.
- (25) Comba, P.; Remenyi, R. *Coord. Chem. Rev.* **2003**, *238*–239, 9–20.
- (26) Comba, P.; Müller, V.; Remenyi, R. *J. Inorg. Biochem.* **2004**, *98*, 896–902.
- (27) Comba, P.; Kerscher, M. *Coord. Chem. Rev.* **2009**, *293*, 564–574.
- (28) Deeth, R. J.; Randell, K. *Inorg. Chem.* **2008**, *47*, 7377–7388.
- (29) Diedrich, C.; Deeth, R. J. *Inorg. Chem.* **2008**, *47*, 2494–2506.
- (30) Deeth, R. J.; Anastasi, A.; Diedrich, C.; Randell, K. *Coord. Chem. Rev.* **2009**, *293*, 795–812.
- (31) Solomon, E. I.; Lever, A. B. P. *Inorganic Electronic Structure and Spectroscopy*; John Wiley & Sons: New York, 1999.
- (32) Solomon, E. I.; Szilagyi, K. R.; George, S. D.; Basumallick, L. *Chem. Rev.* **2004**, *104*, 419–458.
- (33) Solomon, E. I. *Inorg. Chem.* **2006**, *45*, 8012–8025.
- (34) Sarangi, R.; Gorelsky, S. I.; Basumallick, L.; Hwang, H. J.; Pratt, R. C.; Stack, T. D. P.; Lu, Y.; Hodgson, K. O.; Hedman, B.; Solomon, E. I. *J. Am. Chem. Soc.* **2008**, *130*, 3866–3877.
- (35) De Kerpel, J. O. A.; Ryde, U. *Proteins: Struct., Funct., Genet.* **1999**, *36*, 157–174.
- (36) De Kerpel, J. O. A.; Pierloot, K.; Ryde, U. *J. Phys. Chem. B* **1999**, *103*, 8375–8382.
- (37) Ryde, U.; Olsson, M. H. M. *Int. J. Quantum Chem.* **2001**, *81*, 335–347.
- (38) Ryde, U.; Olsson, M. H. M.; Roos, B. O.; Borin, A. C. *Theor. Chem. Acc.* **2001**, *105*, 452–462.
- (39) Siegbahn, P. E. M.; Blomberg, M. R. A. *Chem. Rev.* **2000**, *100*, 421–437.
- (40) Siegbahn, P. E. M. *Q. Rev. Biophys.* **2003**, *36*, 91–145.
- (41) Siegbahn, P. E. M. *Adv. Inorg. Chem.* **2004**, *56*, 101–125.
- (42) Shuku, T.; Sugimori, K.; Sugiyama, A.; Nagao, H.; Sakurai, T.; Nishikawa, K. *Polyhedron* **2005**, *24*, 2665–2670.
- (43) Sugimori, K.; Shuku, T.; Sugiyama, A.; Nagao, H.; Sakurai, T.; Nishikawa, K. *Polyhedron* **2005**, *24*, 2671–2675.
- (44) Bassan, A.; Blomberg, M. R. A.; Siegbahn, P. E. M.; Que, L. Jr. *Angew. Chem.*, **2005**, *44*, 2939–2941.
- (45) Siegbahn, P. E. M.; Borowski, T. *Acc. Chem. Res.* **2006**, *39*, 729–738.
- (46) Siegbahn, P. E. M. *Inorg. Chem.* **2008**, *47*, 1779–1786.
- (47) Swart, M.; *Density Functional Theory Applied to Copper Proteins*; Ph.D. Thesis; Rijksuniversiteit Groningen: Groningen, 2002.
- (48) van den Bosch, M.; Swart, M.; Snijders, J. G.; Berendsen, H. J. C.; Mark, A. E.; Oostenbrink, C.; van der Gunstern, W. F.; Canters, G. W. *ChemBioChem* **2005**, *6*, 738–746.
- (49) Cascella, M.; Magistrato, A.; Tavernelli, I.; Carloni, P.; Rothlisberger, U. *Proc. Natl. Acad. Sci. U.S.A.* **2006**, *103*, 19641–19646.
- (50) Cascella, M.; Cuendet, M. A.; Tavernelli, I.; Rothlisberger, U. *J. Phys. Chem. B* **2007**, *111*, 10248–10252.
- (51) Senn, H. M.; Thiel, W. *Angew. Chem., Int. Ed.* **2009**, *48*, 1198–1229.
- (52) Vreven, T.; Frisch, M. J.; Kudin, K. N.; Schlegel, H. B.; Morokuma, K. *Mol. Phys.* **2006**, *104*, 701–714.
- (53) Vreven, T.; Byun, K. S.; Komaromi, I.; Dapprich, S.; Montgomery, J. A., Jr.; Morokuma, K.; Frisch, M. J. *J. Chem. Theory Comput.* **2006**, *2*, 815–826.

- (54) Lundberg, M.; Morokuma, K. *J. Phys. Chem. B* **2007**, *111*, 9380–9389.
- (55) Datta, S. N.; Sudhamsu, J.; Pandey, A. *J. Phys. Chem. B* **2004**, *108*, 8007–8016.
- (56) Barone, V.; De Rienzo, F.; Langella, E.; Menziani, M. C.; Rega, N.; Sola, M. *Proteins: Struct., Funct., Bioinf.* **2006**, *62*, 262–269.
- (57) Li, H.; Webb, S. P.; Ivanic, J.; Jensen, J. H. *J. Am. Chem. Soc.* **2004**, *126*, 8010–8019.
- (58) Adam, E. T. *Adv. Protein Chem.* **1991**, *42*, 145–149.
- (59) van Gastel, M.; Coremans, J. W. A.; Sommerdijk, H.; van Hemert, M. C.; Groenen, E. J. J. *J. Am. Chem. Soc.* **2002**, *124*, 2035–2041.
- (60) Lu, Y.; Berry, S. M.; Pfister, T. D. *Chem. Rev.* **2001**, *101*, 3047–3080.
- (61) Berry, S. M.; Gieselmann, M. D.; Nilges, M. J.; van der Donk, W. A.; Lu, Y. *J. Am. Chem. Soc.* **2002**, *124*, 2084–2085.
- (62) Berry, S. M.; Ralle, M.; Low, D. W.; Blackburn, N. J.; Lu, Y. *J. Am. Chem. Soc.* **2003**, *125*, 8760–8768.
- (63) Lu, Y. *Angew. Chem., Int. Ed.* **2006**, *45*, 5588–5601.
- (64) Garner, D. K.; Vaughan, M. D.; Hwang, H. J.; Savelleff, M. G.; Berry, S. M.; Honek, J. F.; Lu, Y. *J. Am. Chem. Soc.* **2006**, *128*, 15608–15617.
- (65) Nar, H.; Messerschmidt, A.; Huber, R.; van de Kamp, M.; Canters, G. W. *J. Mol. Biol.* **1991**, *221*, 765–772.
- (66) Borger, B.; Guttschank, J.; Suter, D.; Thomson, A. J.; Bingham, S. J. *J. Am. Chem. Soc.* **2001**, *123*, 2334–2339.
- (67) Remenyi, C.; Reviakine, R.; Kaupp, M. *J. Phys. Chem. B* **2007**, *111*, 8290–8304.
- (68) Sinnecker, S.; Neese, F. *J. Comput. Chem.* **2006**, *27*, 1463–1475.
- (69) Romling, U.; Karen, D.; Schmidt Tummller, B. *FEMS Microbiol. Lett.* **1997**, *150*, 149–156.
- (70) Nelson, D. L.; Cox, M. M. *Lehninger Principles of Biochemistry*; Macmillan Publications: New Delhi, 2000.
- (71) Bizzarri, A. R.; Brunori, E.; Bonanni, B.; Cannistraro, S. *J. Mol. Recognit.* **2007**, *20*, 122–131.
- (72) Dennison, C. *Coord. Chem. Rev.* **2005**, *249*, 3025–3054.
- (73) Li, C.; Yanagisawa, S.; Martins, B. M.; Messerschmidt, A.; Banfield, M. J.; Dennison, C. *Proc. Natl. Acad. Sci. U.S.A.* **2006**, *103*, 7258–7263.
- (74) Li, C.; Banfield, M. J.; Dennison, C. *J. Am. Chem. Soc.* **2007**, *129*, 709–718.
- (75) Dennison, C. *Nat. Prod. Rep.* **2008**, *25*, 15–24.
- (76) Sato, K.; Li, C.; Salard, I.; Thompson, A. J.; Banfield, M. J.; Dennison, C. *Proc. Natl. Acad. Sci. U.S.A.* **2009**, *106*, 5616–21.
- (77) Rajapandian, V.; Sundar Raman, S.; Hakkim, V.; Parthasarathy, R.; Subramanian, V. *J. Mol. Struct. (THEOCHEM)* **2009**, *907*, 1–8.
- (78) Rajapandian, V.; Hakkim, V.; Subramanian, V. *J. Phys. Chem. A* **2009**, *113*, 8615–8625.
- (79) Becke, A. D. *Phys. Rev. A* **1988**, *38*, 3098.
- (80) Becke, A. D. *J. Chem. Phys.* **1993**, *98*, 1372.
- (81) Becke, A. D. *J. Chem. Phys.* **1993**, *98*, 5648.
- (82) Lee, C.; Yang, W.; Parr, R. G. *Phys. Rev. B* **1988**, *37*, 785–789.
- (83) Bonander, N.; Vanngard, T.; Tsai, L. C.; Langer, V.; Nar, H.; Sjolin, L. *Proteins: Struct., Funct., Genet.* **1997**, *27*, 385–394.
- (84) Moratal, J. M.; Romero, A.; Salgado, J.; Perales-Alargón, A.; Jimenez, H. R. *Eur. J. Biochem.* **1995**, *228*, 653–657.
- (85) Hehre, W. J.; Radom, L.; Schleyer, P. V. R.; Pople, J. A. *Ab Initio Molecular Orbital Theory*; Wiley-Interscience: New York, 1986.
- (86) Frisch, M. J.; Trucks, G. W.; Schlegel, H. B.; Scuseria, G. E.; Robb, M. A.; Cheeseman, J. R.; Montgomery, J. A., Jr.; Vreven, T.; Kudin, K. N.; Burant, J. C.; Millam, J. M.; Iyengar, S. S.; Tomasi, J.; Barone, V.; Mennucci, B.; Cossi, M.; Scalmani, G.; Rega, N.; Petersson, G. A.; Nakatsuji, H.; Hada, M.; Ehara, M.; Toyota, K.; Fukuda, R.; Hasegawa, J.; Ishida, M.; Nakajima, T.; Honda, Y.; Kitao, O.; Nakai, H.; Klene, M.; Li, X.; Knox, J. E.; Hratchian, H. P.; Cross, J. B.; Bakken, V.; Adamo, C.; Jaramillo, J.; Gomperts, R.; Stratmann, R. E.; Yazyev, O.; Austin, A. J.; Cammi, R.; Pomelli, C.; Ochterski, J. W.; Ayala, P. Y.; Morokuma, K.; Voth, G. A.; Salvador, P.; Dannenberg, J. J.; Zakrzewski, V. G.; Dapprich, S.; Daniels, A. D.; Strain, M. C.; Farkas, O.; Malick, D. K.; Rabuck, A. D.; Raghavachari, K.; Foresman, J. B.; Ortiz, J. V.; Cui, Q.; Baboul, A. G.; Clifford, S.; Ciosowski, J.; Stefanov, B. B.; Liu, G.; Liashenko, A.; Piskorz, P.; Komaromi, I.; Martin, R. L.; Fox, D. J.; Keith, T.; Al-Laham, M. A.; Peng, C. Y.; Nanayakkara, A.; Challacombe, M.; Gill, P. M. W.; Johnson, B.; Chen, W.; Wong, M. W.; Gonzalez, C.; Pople, J. A. *Gaussian 03*, revision E.01; Gaussian, Inc.: Wallingford, CT, 2003.
- (87) Cambridge Crystallographic Data Centre: <http://www.ccdc.cam.ac.uk> (accessed February 10, 2010). The van der Waals radii (vdW) are taken from the following: (a) Bondi, A. *J. Phys. Chem.* **1964**, *68*, 441–451. (b) Bondi, A. *J. Phys. Chem.* **1966**, *70*, 3006–3007.
- (88) Batsanov, S. S. *Inorg. Mater.* **2001**, *37*, 871–885.
- (89) Case, D. A.; Darden, T. A.; Cheatham, T. E., III; Simmerling, C. L.; Wang, J.; Duke, R. E.; Luo, R.; Crowley, M.; Walker, R. C.; Zhang, W.; Merz, K. M.; Wang, B.; Hayik, S.; Roitberg, A.; Seabra, G.; Kolossváry, I.; Wong, K. F.; Paesani, F.; Vanicek, J.; Wu, X.; Brozell, S. R.; Steinbrecher, T.; Gohlke, H.; Yang, L.; Tan, C.; Mongan, J.; Hornak, V.; Cui, G.; Mathews, D. H.; Seetin, M. G.; Sagui, C.; Babin, V.; Kollman, P. *AMBER 10*; University of California: San Francisco, CA, 2008.
- (90) Duan, Y.; Wu, C.; Chowdhury, S.; Lee, M. C.; Xiong, G.; Zhang, W.; Yang, R.; Cieplak, P.; Luo, R.; Lee, T. *J. Comput. Chem.* **2003**, *24*, 1999–2012.
- (91) Jorgensen, W. L.; Chandrasekhar, J.; Madura, J. D.; Impey, R. W.; Klein, M. L. *J. Chem. Phys.* **1983**, *79*, 926.
- (92) Darden, T.; York, D.; Pedersen, L. *J. Chem. Phys.* **1993**, *98*, 10089–10092.
- (93) Berendsen, H. J. C.; Postma, J. P. M.; van Gunsteren, W. F.; DiNola, A.; Haak, J. R. *J. Chem. Phys.* **1984**, *81*, 3684–3690.
- (94) (a) Uberuaga, B. P.; Anghel, M.; Voter, A. F. *J. Chem. Phys.* **2004**, *120*, 6363–6374. (b) Sindikara, D. J.; Kim, S.; Voter, A. F.; Roitberg, A. E. *J. Chem. Theory Comput.* **2009**, *5*, 1624–1631.
- (95) Ryckaert, J. P.; Cicotti, G.; Berendsen, H. J. C. *J. Comput. Phys.* **1977**, *23*, 327–341.
- (96) Czernuszewicz, R. S.; Fraczkiewicz, G.; Zareba, A. A. *Inorg. Chem.* **2005**, *44*, 5745–5752.
- (97) Fitzpatrick, M. B.; Czernuszewicz, R. S. *J. Biol. Inorg. Chem.* **2009**, *14*, 611–620.
- (98) Kolczak, U.; Salgado, J.; Siegal, G.; Saraste, M.; Canters, G. W. *Biospectroscopy* **1999**, *5*, S19–S32.
- (99) Funk, T.; Kennepohl, P.; Di Bilio, A. J.; Wehbi, W. A.; Young, A. T.; Friedrich, S.; Arenholz, E.; Gray, H. B.; Cramer, S. P. *J. Am. Chem. Soc.* **2004**, *126*, 5859–5866.
- (100) Paraskevopoulos, K.; Sundararajan, M.; Surendran, R.; Hough, M. A.; Eady, R. R.; Hillier, I. H.; Hasnain, S. S. *Dalton Trans.* **2006**, 3067–3076.

JP911301V